Atmos. Chem. Phys., 14, 3307–3323, 2014
www.atmos-chem-phys.net/14/3307/2014/
doi:10.5194/acp-14-3307-2014

Atmospheric Chemistry and Physics Open Access

Investigation of aged aerosols in size-resolved Asian dust storm particles transported from Beijing, China, to Incheon, Korea, using low-*Z* particle EPMA

H. Geng[1], H. Hwang[2], X. Liu[3], S. Dong[4], and C.-U. Ro[5]

[1]Institute of Environmental Science, Shanxi University, Taiyuan 030006, China
[2]Korea Polar Research Institute, Songdo Dong, Yeonsu Gu, 406-840 Incheon, Korea
[3]Chinese Research Academy of Environmental Sciences, Anwai, Beiyuan, Dayangfang 8, Beijing 100012, China
[4]National Research Center for Environmental Analysis and Measurements, No.1 Yuhuinanlu, Chaoyang District, Beijing 100029, China
[5]Department of Chemistry, Inha University, 253 Yonghyun-dong, Nam-gu, 402-751, Incheon, Korea

Correspondence to: C.-U. Ro (curo@inha.ac.kr)

Received: 11 September 2013 – Published in Atmos. Chem. Phys. Discuss.: 29 October 2013
Revised: 8 February 2014 – Accepted: 12 February 2014 – Published: 3 April 2014

Abstract. This is the first study of Asian dust storm (ADS) particles collected in Beijing, China, and Incheon, Korea, during a spring ADS event. Using a seven-stage May impactor and a quantitative electron probe X-ray microanalysis (ED-EPMA, also known as low-*Z* particle EPMA), we examined the composition and morphology of 4200 aerosol particles at stages 1–6 (with a size cut-off of 16, 8, 4, 2, 1, and 0.5 µm in equivalent aerodynamic diameter, respectively) collected during an ADS event on 28–29 April 2005. The results showed that there were large differences in the chemical compositions between particles in sample S1 collected in Beijing immediately after the peak time of the ADS and in samples S2 and S3, which were collected in Incheon approximately 5 h and 24 h later, respectively. In sample S1, mineral dust particles accounted for more than 88 % in relative number abundance at stages 1–5; and organic carbon (OC) and reacted NaCl-containing particles accounted for 24 % and 32 %, respectively, at stage 6. On the other hand, in samples S2 and S3, in addition to approximately 60 % mineral dust, many sea spray aerosol (SSA) particles reacted with airborne SO_2 and NO_x (accounting for 24 % and 14 % on average in samples S2 and S3, respectively), often mixed with mineral dust, were encountered at stages 1–5, and (C, N, O, S)-rich particles (likely a mixture of water-soluble organic carbon with $(NH_4)_2SO_4$ and NH_4NO_3) were abundantly observed at stage 6 (accounting for 68 % and 51 % in samples S2 and S3, respectively). This suggests that an accumulation of sea-salt components on individual ADS particles larger than 1 µm in diameter occurred and many secondary aerosols smaller than 1 µm in diameter were formed when the ADS particles passed over the Yellow Sea. In the reacted or aged mineral dust and SSA particles, nitrate-containing and both nitrate- and sulfate-containing species vastly outnumbered the sulfate-containing species, implying that ambient NO_x had a greater influence on the atmospheric particles than SO_2 during this ADS episode. In addition to partially- or totally-reacted $CaCO_3$, reacted or aged Mg-containing aluminosilicates were observed frequently in samples S2 and S3; furthermore, a student's *t* test showed that both their atomic concentration ratios of [Mg]/[Al] and [Mg]/[Si] were significantly elevated ($P < 0.05$) compared to those in samples S1 (for [Mg]/[Al], 0.34 ± 0.09 and 0.40 ± 0.03 in samples S2 and S3, respectively, vs. 0.24 ± 0.01 in sample S1; for [Mg]/[Si], 0.21 ± 0.05 and 0.22 ± 0.01 in samples S2 and S3, respectively, vs. 0.12 ± 0.02 in sample S1). The significant increase of [Mg]/[Al] and [Mg]/[Si] ratios in Mg-containing aluminosilicates indicates that a significant evolution or aging must have occurred on the ADS particles in the marine atmosphere during transport from China to Korea.

Published by Copernicus Publications on behalf of the European Geosciences Union.

1 Introduction

Asian dust storms (ADSs), called "Ugalz", "Huangsha", "Whangsa", and "Kosa" in Mongolia, China, Korea, and Japan, respectively, occur frequently in the arid and semi-arid areas of Russia, Mongolia, and northern China (Zhang et al., 2010; Natsagdorj et al., 2003). When Asian dust storm episodes occur, the desert dust can be blown eastward by strong winds over thousands of kilometers, being transported widely over eastern China, the Yellow Sea, the Korean Peninsula, Japan Island, and the Pacific Ocean (Feng et al., 2002; Liu et al., 2013). Even the Arctic atmosphere is impacted by long-range transport of Asian dust (Iziomon et al., 2006). In the process of long-range transport, Asian dust is often mixed/reacted with various organic and inorganic materials, making their compositions extremely complicated (Song et al., 2013; Tobo et al., 2010).

The ACE-Asia (Aerosol Characterization Experiments-Asia) and other projects have found that there are substantial modifications in the chemical and physical properties of Asian dust during long-range transport based on detailed measurements of dust aerosols at ground-based, ship, aircraft, and satellite points through "bulk" and individual particle analyses (Huebert et al., 2003; Zhang et al., 2006). Sea spray aerosols (SSAs) mixed internally and externally with mineral dust and the unique reactivity of $CaCO_3$ particles in the atmosphere when Asian dust passes over the sea have been reported (Krueger et al., 2003; Hwang and Ro, 2006; Zhang et al., 2006; Ma, 2010). $CaCO_3$ can neutralize sulfuric and nitric acids (generated by the oxidation of SO_2 and NO_x, respectively) to form hygroscopic sulfates and nitrates (Usher et al., 2003), which often exhibit core-shell structures in "aged" particles (Yuan et al., 2006; Li and Shao, 2009). The formation of sulfate and nitrate coatings or secondary organic matter on minerals, sometimes mixed with SSAs, makes a significant contribution to the optical, chemical, and hygroscopic modification of Asian dust (Bauer et al., 2007; Kojima et al., 2004; Sullivan et al., 2007). This means that Asian dust acts as a significant carrier of pollutants to the downwind locations (Hatch and Grassian, 2008; Choi et al., 2001; Mori et al., 2003; Matsumoto et al., 2006) and the carrying ability is dependent to a large extent on the size, shape, and chemical components of the dust aerosols (Ma et al., 2004; Nie et al., 2012; Wang et al., 2013).

For the detailed characterization of the complex mixtures of atmospherically-processed Asian dust aerosols, many analytical techniques have been utilized, in which the quantitative energy-dispersive electron probe X-ray microanalysis (ED-EPMA, also called low-Z particle EPMA) has proven to be a powerful and useful tool with a relatively short sampling time and without a complicated sample pretreatment process (Hwang and Ro, 2005, 2006; Geng et al., 2009a, 2011a, b). This single-particle analytical technique, which is based on scanning electron microscopy (SEM) coupled with an ultra-thin window energy-dispersive X-ray spectrometry (EDX), can simultaneously detect the morphology and constituent elements of an individual particle and provide information on the aging process and transformation of many environmentally-important particles, such as nitrates, sulfates, and carbonaceous species (Maskey et al., 2010; Choël et al., 2005, 2007). For instance, through the application of low-Z particle EPMA to characterize airborne particle samples collected in the marine boundary layer (MBL) of the Bohai Sea and Yellow Sea on 30 April–1 May 2006, Geng et al. (2009a) suggested that Asian dust aerosols are important carriers of gaseous inorganic nitrogen species, especially NO_x and NH_3. Recently, the combined use of low-Z particle EPMA with attenuated total reflection Fourier transform infrared (ATR-FTIR) imaging technique and Raman microspectrometry (RMS) demonstrated that many individual Asian dust particles were extensively chemically-modified and highly complicated in compositions (Song et al., 2013; Sobanska et al., 2012).

In the present study, low-Z particle EPMA was used to examine how size-resolved Asian dust contributes to ambient particulate matter in Beijing, China, and Incheon, Korea, due to an ADS event that occurred in April 2005 and to examine the heterogeneous aging of Asian dust particles when they transported from China to Korea over the Yellow Sea. This study presents the detailed characterization of reacted or aged mineral dust and SSAs, which became physically and chemically altered through interactions with anthropogenic gaseous pollutants and marine aerosols. Special emphasis was placed on quantitative analysis of the elemental percentages of reacted particles in the size range of 0.2–10 µm. The changes in the ratios of [Cl] / [Na], [Cl] / [N], and [Cl] / [S] in the reacted or aged SSAs and the changes of [Mg] / [Al] and [Mg] / [Si] ratios in the reacted or aged aluminosilicates were investigated. To the best of the authors' knowledge, this is the first report of the results for ADS particles collected in Beijing and Incheon during the same spring ADS episode. The intent of this investigation of the chemical compositions of size-resolved ADS particles collected at the two sites and identification of reacted or aged aerosols is to help improve the understanding of the sources, reactivity, transport, and removal of mineral dust particles.

2 Materials and methods

2.1 Sampling sites and dates

The two sampling sites were located in Beijing, China, and Incheon, Korea (Fig. 1). In Beijing, immediately after the peak of the ADS event on 28 April 2005, aerosols were collected on the roof of a building at the Chinese Research Academy of Environmental Sciences (39.98° N, 116.42° E), approximately 30 m a.g.l. (notated as sample S1 hereafter; Table 1). Approximately 5 and 24 h later, samplings were conducted on the roof of a five-story building (approximately

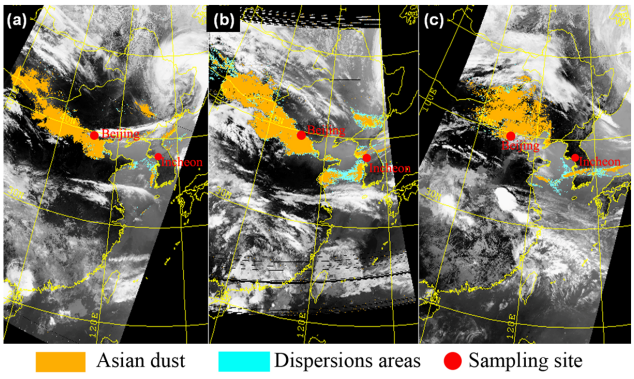

Fig. 1. Satellite images recorded **(a)** at 11:50 Korea Standard Time (KST) on 28 April 2005; **(b)** at 18:55 KST on 28 April 2005; and **(c)** at 11:45 KST on 29 April 2005 (provided by NOAA).

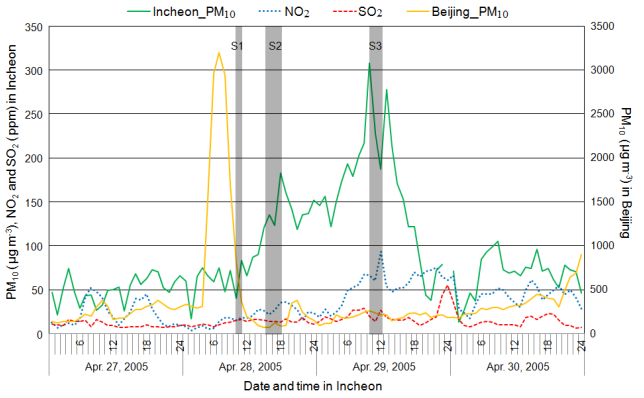

Fig. 2. Hourly values of PM_{10} (in $\mu g\,m^{-3}$), NO_2 and SO_2 concentrations (in ppm) recorded in Incheon (left axis) and hourly values of PM_{10} (in $\mu g\,m^{-3}$) recorded in Beijing (right axis) from 27 to 30 April 2005. The shadowed areas correspond (left to right) to the sampling times of the aerosol samples S1, S2, and S3. Sample S1 was collected in Beijing, China, while samples S2 and S3 were collected in Incheon, Korea.

25 m a.g.l.) at Inha University (37.45° N, 126.73° E), Incheon. The first sampling in Incheon was carried out at 15:00–18:55 (KST) on 28 April 2005 when the ADS event began (sample S2) and the second was at the peak time of the ADS event on 29 April 2005 (sample S3). Figure 2 shows the hourly PM_{10} values recorded in Beijing and Incheon during four consecutive days from 27 to 30 April 2005. In Beijing, the 24 h average PM_{10} concentrations reached 706 $\mu g\,m^{-3}$ on 28 April 2005, which is approximately five times higher than the Chinese state Grade-II standard of 150 $\mu g\,m^{-3}$; and hourly PM_{10} exceeded 1500 $\mu g\,m^{-3}$ for five consecutive hours with the peak level of 3198 $\mu g\,m^{-3}$ (at 07:00 on 28 April 2005, KST). The PM_{10} concentrations in Incheon, which were recorded at an air quality monitoring station (Sungui-dong, Nam-gu) close to the sampling site, exceeded the Korean National Ambient Air Quality Standard (100 $\mu g\,m^{-3}$ on the daily average) with 158 $\mu g\,m^{-3}$ on 29 April 2005. The hourly PM_{10} levels exceeded 100 $\mu g\,m^{-3}$ for 28 consecutive hours and reached up to 308 $\mu g\,m^{-3}$ at the peak time of the ADS episode. The PM_{10} level in Incheon was ten times lower than the maximum value recorded in Beijing due to the dispersion and removal of ADS particles during long-range transport.

The particles were collected on Ag and Al foils, using the seven-stage May cascade impactor. At a flow rate of 20 L min^{-1}, the May impactor has nominal aerodynamic cut-off diameters of 16, 8, 4, 2, 1, 0.5, and 0.25 µm for stages 1–7, respectively. The number–size distribution of ambient particles was monitored in situ using an optical particle counter to observe the particle number concentration. To prevent the overloading of particles at the impaction slots, the sampling durations were adjusted according to the atmospheric particle load, varying between 30 s (for particles on stage 6) and 2 h (for particles on stage 1). The collected samples were placed in Petri dishes, sealed, and stored in a desiccator prior to the measurements.

2.2 Measurement and analysis

The size, morphology, and chemical composition of the individual aerosol particles were determined by a SEM equipped with an Oxford Link SATW ultrathin window EDX detector (Hitachi S-3500N). The resolution of the detector was 133 eV for Mn-Kα X-rays. The X-ray spectra were recorded under the control of INCA software. An accelerating voltage and beam current of 10 kV and 1.0 nA, respectively, were chosen to achieve the optimal experimental conditions, such as low background level and high sensitivity for low-Z element analysis. A typical measuring time of 10 s was used to limit the beam damage on sensitive particles. The secondary electron images (SEIs) and X-ray spectra of 100 particles on stages 1 and 6 and 300 particles on stages 2 to 5, respectively, were detected (1400 particles per sample). In total, 4200 particles were analyzed for the three samples. The particle equivalent diameters were estimated from their projected area, assuming the particles to be spherical. The methods for acquiring the net X-ray intensities of the elements; for simulating the measured X-ray intensities for all chemical elements, in a particle by Monte Carlo calculations; and for using the "expert system" program to perform chemical speciation and determine the particle group distributions are described elsewhere (Vekemans et al., 1994; Ro et al., 2003, 2004). The elemental quantification procedure provided results with an accuracy of within 12 % relative deviations between the calculated and nominal elemental concentrations for various standard particles (Ro et al., 2000, 2001).

Table 1. Sampling locations, dates and times.

Samples	Sampling locations	Date	Time sampling began (UTC)	Local time of sampling (KST)	Sampling conditions
Sample S1	Beijing, China	28 Apr 2005	00:45	09:45–11:00	Just after the peak time of ADS in Beijing
Sample S2	Incheon, Korea	28 Apr 2005	06:00	15:00–18:55	At the onset of ADS in Incheon
Sample S3	Incheon, Korea	29 Apr 2005	00:25	09:25–11:45	At the peak time of ADS in Incheon

2.3 Backward trajectories for air mass transport history

The 48 h backward air mass trajectories at receptor heights of 500 m, 1000 m, and 2000 m a.s.l. were produced using the HYbrid Single-Particle Lagrangian Integrated Trajectory model available at the NOAA Air Resources Laboratory's web server (http://ready.arl.noaa.gov/HYSPLIT.php). As shown in Figs. 1 and 3, the dust cloud, which originated from Mongolia (likely from the Gobi Desert), moved over Inner Mongolia and Beijing city, China, and was dispersed southeast toward the Korean Peninsula.

3 Results and discussion

3.1 Particle size on different collecting stages

The particle size is closely related to the chemical compositions, heterogeneous reactivity, and ultimate fate of ambient particles (Formenti et al., 2011). The mean equivalent diameters of all 4200 particles analyzed in stages 1–6 are 15.6 ± 7.0, 7.5 ± 2.6, 3.8 ± 1.4, 2.3 ± 1.0, 1.3 ± 0.6, 0.9 ± 0.6 µm in size, respectively (Table 2), which have minor deviation compared to the nominal aerodynamic cut-off diameters of the May impactors (with 50 % efficiency of 16, 8, 4, 2, 1, and 0.5 µm for stages 1–6, respectively). The particles on stage 6 in sample S1 were significantly smaller than those in both samples S2 and S3 because many hygroscopic particles, which look dark and "big" in size on their SEIs, were encountered on stage 6 of samples S2 and S3 (Figs. 4 and 5). Also, a lot of hygroscopic particles were encountered on stage 4 of samples S2 and S3 (Fig. 6).

The particle size changed during mixing among the different types of particles. As illustrated in Fig. 4, the particles on stage 1 had a similar distribution trend in samples S1–S3, but for the particles on stages 2 and 3, those in sample S1 (i.e., Beijing particles) tended to be larger than those in samples S2 and S3 (i.e., Incheon particles) because the S1 particles had lower percentages in the smaller size range ($\sim$ 21 % in the size range of 4–6 µm in diameter for stage 2 and 2–3 µm for stage 3 compared to more than 40 % in those size ranges in samples S2 and S3). The trend was opposite for the particles on stages 4 and 6. The particles on stages 4 and 6 in sample S1 had a higher percentage in the smaller size range than those in samples S2 and S3 ($\sim$ 70 % vs. 40 % in the 1–2 µm size range for stage 4 and 90 % vs. 60 % in 0.1–1 µm size range for stage 6). This suggests that the smaller particles collected in Incheon tended to become larger due likely to mixing between particles (e.g., dust particles mixed with SSAs) or reactions between particles and gas/liquid substances (e.g., dust particles reacted with NO_x and SO_2). These mixing and/or reaction processes would lead to chemical modification of particles at different size ranges, as shown in Figs. 7 and 8.

3.2 Classification of measured particles

The way used to determine the chemical species of individual particles and perform a classification based on their chemical species is summarized briefly here. Firstly, the particles were regarded to be composed of just one chemical species when the chemical species constituted at least 90 % of the atomic fraction. Secondly, efforts were made to determine the chemical species of the internally mixed particles based on all the chemical species identified. Thirdly, elements with less than 1 at. % were neglected in the chemical speciation because elements at such trace levels cannot be investigated reliably. The speciated particles were grouped into different types according to the criteria summarized in Table 3. Overall, ten groups of particles were classified: (1) unreacted mineral dust, (2) aged or reacted mineral dust, (3) fresh or unreacted SSA (or NaCl-containing), (4) reacted or aged SSA (and mixtures) or reacted NaCl-containing particles, (5) carbon-rich particles, (6) organic carbon (OC) particles, (7) (C, N, O, S)-rich particles, (8) K-containing particles, (9) Fe-rich particles, and (10) others. Some SEIs of various types of particles are shown in Figs. 5 and 6.

Table 2. Mean equivalent diameters (μm) of the particles analyzed at different stages.

Samples	Stage 1 ($n = 300$)	Stage 2 ($n = 900$)	Stage 3 ($n = 900$)	Stage 4 ($n = 900$)	Stage 5 ($n = 900$)	Stage 6 ($n = 300$)
S1	15.6 ± 7.0	8.2 ± 2.5	4.3 ± 1.4	1.7 ± 0.7	1.3 ± 0.5	0.4 ± 0.2
S2	15.3 ± 6.9	7.2 ± 2.6	3.7 ± 1.4	2.7 ± 0.9	1.3 ± 0.6	0.9 ± 0.3
S3	16.0 ± 7.3	7.0 ± 2.6	3.5 ± 1.3	2.5 ± 1.0	1.4 ± 0.7	1.4 ± 0.6
Mean	15.6 ± 7.0	7.5 ± 2.6	3.8 ± 1.4	2.3 ± 1.0	1.3 ± 0.6	0.9 ± 0.6

Units are μm; n denotes the number of analyzed particles.

3.3 Chemical compositions of size-resolved particles in samples S1, S2, and S3

3.3.1 Particles on stages 1–5

Overall, 3900 particles on stages 1–5 of samples S1–S3 (1300 for each sample) were analyzed. Based on the classification of the particles, the relative number abundances of the various particle types were obtained by dividing the number of a specific type of particle by the total number of particles analyzed for each stage, as shown in Figs. 7 and 8. It was found that there were significant differences in the aerosol components among the three samples by comparing the relative abundances of the major particle types at different size ranges, reflecting the aging process of the ADS particles. A detailed description of the changes in the relative abundances of the various types of particles is summarized as follows.

Mineral dust particles

Mineral dust particles appeared irregular and bright on their SEIs. The typical unreacted mineral dust particles included aluminosilicate, quartz (SiO_2), calcite ($CaCO_3$), dolomite ($CaMg(CO_3)_2$), and TiO_2 (Shao et al., 2008). The reacted or aged mineral dust particles mainly included "reacted $CaCO_3$ / $CaMg(CO_3)_2$" and "aluminosilicate + (N, S)", where the (N, S) notation represents compounds containing either nitrates, sulfates, or both. They were either produced when mineral dust particles (particularly Ca-containing species) react with airborne SO_2 and NO_x in the presence of moisture or with "secondary acids" such as H_2SO_4, HNO_3, and HCl (Harris et al., 2012; Wang et al., 2005), or were formed from the adsorption of NH_4NO_3 and/or $(NH_4)_2SO_4$ / NH_4HSO_4 on the particle surface (Sullivan et al., 2007). In the present study, the overall relative abundance of mineral dust particles was more than 88 % of the particles analyzed for sample S1 collected in Beijing. On the other hand, for samples S2 and S3 collected in Incheon, the relative abundances of mineral dust particles were smaller than that of sample S1. The mixture of reacted SSA and mineral dust, which was not encountered in sample S1, was frequently observed in samples S2 and S3. Overall, the reacted (aged) mineral dust particles were of greater relative abundance than the unreacted ones on stages 1–5: approximately 71 % vs. 17 % on average for sample S1; 50 % vs. 6 % for sample S2; and 48 % vs. 13 % for sample S3 (Fig. 7). Furthermore, the majority of aged mineral dust particles were nitrate-containing species and both sulfate- and nitrate-containing species (Tables 4 and 5), consistent with the results for aerosol particles collected in the marine-atmospheric boundary layer of the Yellow Sea when an ADS has passed by (Geng et al., 2009a). In sample S1, the relative abundance of the reacted $CaCO_3$ or $CaMg(CO_3)_2$ was 3 %, which was similar to that of the unreacted ones (4 %). On the other hand, in samples S2 and S3, the reacted $CaCO_3$ or $CaMg(CO_3)_2$ largely outnumbered the unreacted ones (13 % vs. 1 % in sample S2 and 11 % vs. 2 % in sample S3). The lower relative abundance of reacted $CaCO_3$ or $CaMg(CO_3)_2$ in sample S1 than in samples S2 and S3 suggests that some atmospheric reactions occurred on the surface of $CaCO_3$ or $CaMg(CO_3)_2$ particles when they passed over the Yellow Sea (Fairlie et al., 2010; Ma et al., 2004; Wang et al., 2005). Possibly, moisture over the sea might play important roles in facilitating the reactions of $CaCO_3$ or $CaMg(CO_3)_2$ with NO_x and SO_2 (Formenti et al., 2011).

The aluminosilicate particles with strong X-ray peaks of Al, Si, and O and minor elements, such as Na, K, Ca, Mg, Fe, Cl, Ti, etc., are important components of mineral dust. They exist in many different forms, including Na-feldspar, K-feldspar, muscovite, montmorillonite, illite, Mg-vermiculite, kaolinite, talc, pyrophyllite, etc. (Jung et al., 2010; Malek et al., 2011). Most of them belong to clay mineral. Table 5 lists the elemental compositions of different types of aluminosilicates and their respective relative abundances. The reacted or aged aluminosilicates greatly outnumbered the unreacted ones in all three samples (on average, 58 % vs. 12 % in sample S1, $\sim$ 4.8 fold; 33 % vs. 3 % in sample S2, $\sim$ 11 fold; and 35 % vs. 8 % in sample S3, $\sim$ 4.4 fold), where most aged aluminosilicates contained nitrates. Those containing only sulfates without nitrates were rarely encountered, indicating that aluminosilicate particles react more easily with NO_2 or HNO_3 than with SO_2 or H_2SO_4. NH_4NO_3 adsorbed on the surface of aluminosilicate particles cannot be excluded.

Many aluminosilicate particles contain magnesium (Mg). The Mg-containing species in unreacted aluminosilicates accounted for 73 %, 46 %, and 40 % in samples S1–S3,

Table 3. Classification of the aerosol particles based on their SEIs and X-ray spectral data.

Particle type	Characteristics and possible compositions	
1. Unreacted mineral dust	Aluminosilicate	Irregular and bright, having strong Al, Si, and O peaks, often with minor elements, such as Na, Mg, S, Cl, K, Ca, and Fe
	SiO_2	Irregular and bright, having strong Si and O signals in its X-ray spectrum (the atomic concentration ratio of Si and O is around 1:2)
	$CaCO_3$, $MgCO_3$, and $CaMg(CO_3)_2$	Appearing irregular and bright, with strong C, O, Ca and/or Mg signals in its X-ray spectrum
	TiO_2	Appearing irregular and bright, having strong Ti and O signals in its X-ray spectrum
2. Reacted (or aged) mineral dust	Aged or reacted aluminosilicate, $CaCO_3$, $CaMg(CO_3)_2$, etc., with SO_2 and NO_x or with "secondary acids" such as H_2SO_4 and HNO_3	Irregular and bright on their SEIs, sometimes enclosed or mixed with dark droplet, having N and/or S peaks in X-ray spectra, indicating either nitrates, sulfates, or both are generated on their surface
3. Fresh sea spray aerosol (SSA) or NaCl-containing particles	(Na, Mg)Cl-containing	Cubic and bright, with predominant Na and Cl signals and minor C, O, Mg, etc.
4. Reacted (or aged) NaCl-containing or SSA particles	Nitrate-containing Sulfate-containing Both nitrate- and sulfate-containing Aged SSA mixed with mineral dust	Covered or enclosed with liquid, containing NO_3^- and/or SO_4^{2-} in addition to Na, Cl, and Mg, sometimes with detectable Al and Si and/or Ca signals
5. Carbon-rich particles	Soot aggregates, tar ball, char or coal dust	The sum of the C and O concentration is more than 90 at. %, and the concentration of C is much larger (generally more than 3 times) than that of O, and almost no other element is present
6. Organic carbon (OC) particles		Irregular and solid particles, or dark droplets, with more than 90 at. % of C, O, and sometimes N (concentration of C is not much larger than that of O)
7. (C,N,O,S)-rich particles	$(NH_4)_2SO_4$ / NH_4HSO_4-containing particles, perhaps mixed with NH_4NO_3	C, N, O, and S (sometimes just C, O, and S) peaks are obvious, with a lot of water-soluble organic matters inside
8. K-containing particles	Particles containing KCl and/or K_2SO_4	Irregular and bright, with K, O, S, and/or Cl peaks in their X-ray spectra
9. Fe-rich particles	FeO_x or $Fe(OH)_x$	Usually contain more than 20 at. % of Fe, generally in the form of iron ((oxy)hydr)oxides, often with minor amounts of C, Si, and Al
10. Others		Irregular and bright on their SEIs, only containing O or Cl

Table 4. Relative number abundance of unreacted and reacted $CaCO_3$ / $CaMg(CO_3)_2$ in samples S1–S3.

Type	Relative abundance (%) in sample S1					Relative abundance (%) in sample S2					Relative abundance (%) in sample S3				
	st1	st2	st3	st4	st5	st1	st2	st3	st4	st5	st1	st2	st3	st4	st5
1. Unreacted $CaCO_3$ or $CaMgCO_3$	8	4	4	4	1	2	1	0	2	0	10	0	0	0	0
2. Reacted $CaCO_3$ or $CaMgCO_3$	2	3	5	2	4	11	18	17	12	6	15	12	17	7	1
Nitrate-containing	1	3	4	2	3	11	7	3	2	1	5	5	0	0	0
Sulfate-containing	0	0	1	0	0	0	1	5	0	1	8	4	9	5	1
Both-containing	1	0	0	0	1	0	10	9	10	4	2	3	8	2	0
3. Sum of $(1+2)$	10	7	9	6	5	13	19	17	14	6	25	12	17	7	1

respectively, on average; and in the reacted or aged aluminosilicates, they accounted for 74 %, 63 %, and 63 % in samples S1-S3, respectively. Corresponding to the mineralogy, the particles with X-ray peaks of Al, Si, O, and Mg in the EDX spectra are considered as amesite or allophite, normally associated with chlorite, magnetite, rutile, diaspore, calcite, grossular, diopside, and clinozoisite in a range of locations. The particles showing strong X-ray peaks for Al, Si, O, Mg, and Fe might be a Mg-vermiculite, likely being formed by weathering or hydrothermal alterations of iron-bearing phlogopite and annite (Malek et al., 2011). In addition, Mg signals can also be observed in illite and montmorillonite. They have been commonly observed in airborne particles collected during ADS events (Xuan et al., 2004; Schulz et al., 2012; Sobanska et al., 2012). These Mg-containing aluminosilicates are abundant in the soils of Chinese loess areas and desert areas (Malek et al., 2011; Takahashi et al., 2010). Therefore, it is expected that they would be uplifted into the air and transported to downwind locations by strong winds when an ADS occurs. Herein, they were simplified as the groups of (Al, Si, O, Mg) and (Al, Si, O, Mg) and mixture, in which the mixture included one or more of Na, Fe, Ca, K, Cl, P, and Ti (Table 5). The relative abundance of Mg-containing aluminosilicates (AlSiOMg and AlSiOMg/mixture species) in Beijing was larger than that in Incheon (on average, 73.8 % in sample S1 vs. 54.6 % and 51.8 % in samples S2 and S3). Moreover, the calculated atomic concentration ratios showed an obvious increase in [Mg] / [Al] and [Mg] / [Si] in samples S2 and S3 compared to sample S1, for both the unreacted and reacted (aged) aluminosilicate particles (Fig. 9). In particular, for the reacted (aged) aluminosilicate particles, the student's *t* test showed that their atomic concentration ratios of [Mg] / [Al] and [Mg] / [Si] were significantly elevated ($P < 0.05$) (for [Mg] / [Al], 0.34 ± 0.09 and 0.40 ± 0.03 in samples S2 and S3, respectively, vs. 0.24 ± 0.01 in sample S1; for [Mg] / [Si], 0.21 ± 0.05 and 0.22 ± 0.01 in samples S2 and S3, respectively, vs. 0.12 ± 0.02 in sample S1). The significant increase of [Mg] / [Al] and [Mg] / [Si] ratios in reacted Mg-containing aluminosilicates indicates that aging occurred on the mineral dust during ADS particles' dispersion from China to Korea in the marine atmosphere. It implies that Mg-containing aluminosilicates played important roles in the heterogeneous aging process of mineral dust when they passed over the Yellow Sea. The internal mixture of mineral dust and SSAs by collision or coagulation may have contributed to the increase of [Mg] / [Al] and [Mg] / [Si] ratios in Mg-containing aluminosilicates. Why and how the reactions happened will be discussed in the Sect. 3.4.

Sea spray aerosols (SSAs)

Figure 10 shows the relative abundances of fresh and reacted (aged) SSAs at stages 1–5. As no SSA was encountered in sample S1, SSAs in samples S2 and S3 likely originated from the Yellow Sea. The fresh SSA particles, which were identified by the presence of Na and Cl peaks and often with minor C, O, Mg, and Ca signals in their X-ray spectra, were encountered only in sample S2 (none were observed in sample S3) with low abundance: less than 1 % on stage 2, stage 4, and stage 5. On the other hand, many aged or reacted SSA particles were encountered in samples S2 and S3 (approximately 24 % and 14 % in samples S2 and S3, respectively), suggesting that the aerosols were largely influenced by airborne NO_x and/or SO_2 in the marine atmosphere.

The reacted or aged SSAs were classified into three types based on their SEIs and X-ray spectral data. The first was for those containing nitrates, such as Na(Cl, NO_3) and (Na, Mg)(Cl, NO_3). The second was for those containing SO_4^{2-} or methanesulfonate ($CH_3SO_3^-$), which were generated from the reactions of SSAs with SO_2 / H_2SO_4 and/or methylsulfonic acid (MSA) from the oxidization of dimethylsulfide (DMS) (Hopkins et al., 2008; Ault et al., 2013). Because the contribution of biologically produced DMS to sea-salt sulfate (ss-SO_4^{2-}) is not significant over the Yellow Sea and Bohai Sea compared to the anthropogenic contributions (Yang et al., 2009), sulfate-containing SSAs generated from oxidized DMS can be neglected. The third was for those containing both NO_3^- and SO_4^{2-} / $CH_3SO_3^-$. Nitrate-containing ones significantly outnumbered the SO_4^{2-} / $CH_3SO_3^-$- and both-containing ones on stages 1–5 (see Fig. 10). In addition, the reacted SSAs mixed internally with mineral dust species

Table 5. Relative number abundances (%) of various types of aluminosilicates in samples S1–S3.

Types based on X-ray signals/mineralogy	Sample S1					Sample S2					Sample S3				
	st1	st2	st3	st4	st5	st1	st2	st3	st4	st5	st1	st2	st3	st4	st5
1. Unreacted aluminosilicates	**13**	**9**	**10**	**12**	**14**	**4**	**4**	**2**	**4**	**3**	**20**	**6**	**8**	**5**	**2**
(1) Al Si O (sometimes with minor Ca, P, or Ti), likely kaolinite	1	1	0	3	0	0	0	0	1	1	2	0	1	1	2
(2) Al Si O Fe, likely almandine	1	0	0	0	0	0	0	0	0	0	1	0	0	0	0
(3) Al Si O K (sometimes with minor Ca, Ti, or Na), likely K-feldspar or illite	2	1	1	0	1	2	0	0	0	0	3	1	1	0	0
(4) Al Si O Na (sometimes with minor Cl, Ca, or Ti), likely Na-feldspar	0	1	1	1	1	1	2	0	0	1	3	1	1	2	0
(5) Al Si O Mg, likely amesite or pyrope	1	1	3	4	7	0	0	0	0	0	3	0	1	0	0
(6) Al Si O Mg/mixture (one or more or all of Na, Fe, Ca, K, Cl, P, and Ti), likely montmorillonite or Mg-vermiculite	8	4	5	4	5	1	1	1	2	1	8	3	3	1	0
2. Reacted aluminosilicates	**40**	**66**	**61**	**66**	**57**	**26**	**35**	**46**	**28**	**31**	**23**	**45**	**40**	**32**	**33**
(1) Nitrate-containing	38	65	61	64	56	20	33	38	25	26	21	41	29	27	19
Al Si O N (sometimes with minor P or Ca)	2	4	3	2	2	1	3	4	5	3	2	1	0	3	5
Al Si O N Fe (sometimes with minor Ti)	5	3	4	3	3	0	0	0	0	0	3	0	0	0	2
Al Si O N K (sometimes with minor Fe or Ca)	1	5	5	3	4	3	1	1	1	0	0	2	0	0	1
Al Si O N Na (sometimes with minor Cl, K, Ca, P, or Fe)	2	6	10	5	3	5	12	5	5	4	4	16	4	7	2
Al Si O N Mg (sometimes with minor Cl, Ca, or K)	7	9	6	20	21	4	1	2	6	1	3	1	0	1	4
Al Si O N Mg/mixture	21	38	33	32	23	7	16	26	9	17	9	21	25	15	5
(2) Sulfate-containing	1	0	0	0	0	1	0	1	0	0	1	0	2	0	0
Al Si O S	0	0	0	0	0	0	0	0	0	0	0	0	1	0	0
Al Si O Mg S/mixture	1	0	0	0	0	1	0	0	0	0	1	0	2	0	0
(3) Both nitrate- and sulfate-containing	1	0	0	1	1	5	2	7	3	4	1	4	9	5	14
Al Si O N S (with minor Na, Fe, Ca, K, P, or Cl but without Mg)	0	0	0	0	1	2	1	2	0	1	0	3	3	1	4
Al Si O N S Mg/mixture (one or more or all of Na, Fe, Ca, K, Cl, P, and Ti)	1	0	0	1	0	3	1	5	3	3	1	2	6	4	10
3. Sum of (1 + 2)	**53**	**75**	**71**	**78**	**71**	**30**	**39**	**47**	**32**	**33**	**43**	**51**	**48**	**37**	**35**
4. Percent of nitrate-containing species in all reacted aluminosilicates	98	100	100	100	99	96	100	99	100	99	96	100	94	99	100
5. Percent of Mg-containing species in the unreacted aluminosilicates	69	63	83	68	83	25	33	81	54	37	55	56	61	27	0
6. Percent of Mg-containing species in the reacted aluminosilicates	75	73	64	81	77	58	52	73	62	69	61	53	81	64	57
7. Mean of (5 + 6)	72	68	74	75	80	42	43	77	58	53	58	55	71	46	29

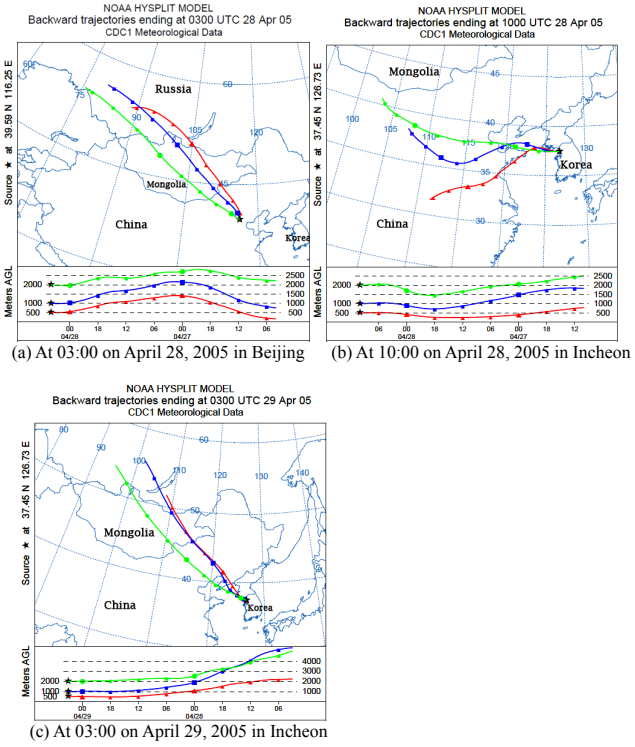

(a) At 03:00 on April 28, 2005 in Beijing (b) At 10:00 on April 28, 2005 in Incheon

(c) At 03:00 on April 29, 2005 in Incheon

Fig. 3. 48 h backward trajectories of air masses ending **(a)** at 03:00 UTC on 28 April 2005 in Beijing; **(b)** at 10:00 UTC on 28 April 2005; and **(c)** at 03:00 UTC on 29 April 2005 in Incheon. Trajectory plots were produced with HYSPLIT from the NOAA ARL website: http://www.arl.noaa.gov/ready/.

(such as $CaCO_3$ and aluminosilicates) were classified into the group of "reacted SSAs and mixture". They were encountered frequently on stages 2–5, accounting for 65 % on average in sample S2 (58 %, 67 %, 68 %, and 67 % in stages 2–5, respectively) and 60 % in sample S3 (71 %, 61 %, 58 %, and 48 % in stages 2–5, respectively), which suggests that the internal mixing of SSAs and mineral dust occurred during the ADS event, mainly after the ADS particles left the continent.

Low-Z particle EPMA can clearly distinguish between partially-reacted and totally-reacted SSAs. The former are observed as nitrates and sulfates of sodium and magnesium with residual chlorine, whereas the later are found in the form of just $(Na,Mg)NO_3$ and/or $(Na,Mg)SO_4$ without Cl being detected in the X-ray spectra (Geng et al., 2009a, b). In particular, this method provides the possibility of quantitative analysis of the elemental percentages in SSAs among different stages and samples. This means that the changes in [Cl] / [Na] ratio, [Cl] / [N] ratio, and [Cl] / [S ratio could reflect the Cl depletion of reacted SSAs to some extent, as shown in Table 6. On average, the ratio of [Cl] / [Na] in the partially-reacted and totally-reacted SSA particles was 0.09 and 0.07 in samples S2 and S3, respectively. The [S] / [Na] ratio in all the reacted or aged SSAs was in the 0.5–1.08 range, largely more than that in seawater: ca. 0.083 (Maskey et al., 2011), implying that ss-SO_4^{2-} accounted for a minor fraction in the reacted SSA particles compared to the non-sea salt sulfate (nss-SO_4^{2-}). In the nitrate-containing reacted SSA particles, the ratio of [N] / [Na] in samples S2 and S3 was ca. 1.14 and 0.88, respectively on average, close to the stoichiometry of $NaNO_3$.

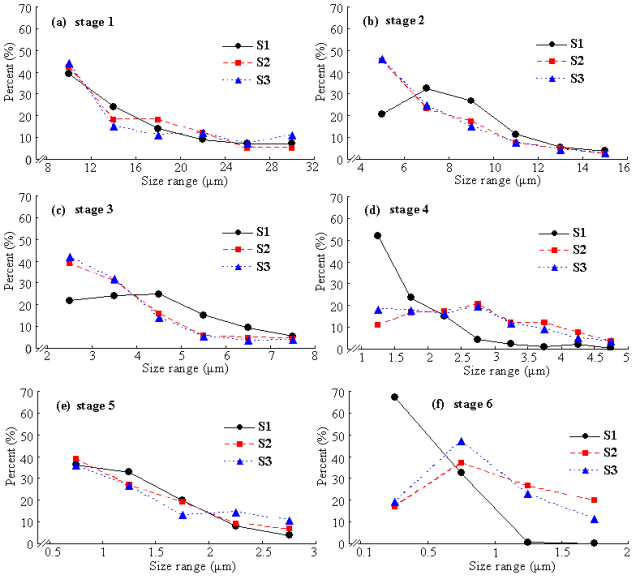

Fig. 4. Size range of analyzed particles on stages 1–6 for samples S1–S3.

Carbonaceous particles

For the ADS particles, carbon-rich particles are in low abundances on stages 1–5 (∼ 2 % on average for each sample) compared to OC particles (7 %, 16 % and 17 % on average for samples S1–S3, respectively) (Fig. 7), suggesting that OC particles are dominant in the carbonaceous aerosols. Furthermore, the abundance of OC particles collected in Incheon outweighs that collected in Beijing (on average, approximately 16 % and 17 % in samples S2 and S3, respectively, vs. 7 % in sample S1), implying that many OC particles in Incheon came from the marine atmosphere over the Yellow Sea during the ADS event. In addition, volatile organic compounds (VOCs), which can condense onto organics during transport, might also contribute to the increase of OC particles in Incheon (Atkinson, 2000; Wang and Zhao, 2008).

(C, N, O, S)-rich particles

The (C, N, O, S)-rich particles were encountered at stage 5 in sample S3. EDX revealed peaks for C, O, S, and N and their SEIs showed round, dark shape. These particles are considered as $(NH_4)_2SO_4$ / NH_4HSO_4-containing particles, a secondary species produced from the reactions of ambient

sulfate or sulfuric acid with ammonia (Geng et al., 2009b). NH_4NO_3, which is formed by a reaction of ambient NO_2 or HNO_3, might be included in this type of particle because the N concentration is much larger than the S concentration in some particles of this type (Fig. 11). These will be described in detail in Sect. 3.3.2 because (C, N, O, S)-rich particles were observed as being abundant in stage 6 samples.

Fe-rich and other particles

Fe-rich particles appeared bright and irregular on their SEIs and normally contained strong Fe and O peaks in their X-ray spectra, sometimes with minor C, Si, and Al. Several of them are shown in Fig. 5 (particles 2, 5, and 41) and Fig. 6 (particle 52). These particle types are often interpreted as goethite, hematite, or magnetite in atmospheric aerosols. They can be from natural sources or human activities such as mining, steel production, metallurgical industries, the abrasion of vehicular brake linings, etc. (Flament et al., 2008). In the present study, Fe-rich particles at stages 1–5 had average abundances of 2 %, 1 %, and 4 % in samples S1–S3, respectively. This means that the ADS did not increase the level of Fe-rich particles significantly in the atmosphere of Incheon.

3.3.2 Particles on stage 6

The compositions of particles on stage 6 and stages 1–5 differed significantly. As shown in Fig. 8, many aged NaCl-containing particles (< 1 µm in diameter) were encountered in sample S1 with an abundance of approximately 32 %. Their morphologies in SEI (particle 3 in Fig. 5a) and the information from the backward air mass trajectory (Fig. 3a) show that they are different from the SSA particles from the Yellow Sea. They look dry and are smaller than SSA particles in size, implying that they are halite from the desert (Okada and Kai, 2004). They might have come from dried salt lakes or saline soils near Hunshandake Sandy Land or Hulunbeier Sandy Land in the southeast and northeast, respectively, of the Inner Mongolia plateau (Zhang et al., 2010; Sun et al., 2010). These halite particles can react with NO_x / HNO_3 during transport and then be transformed to $NaNO_3$. Industrial sources could not be excluded for the dry and fine-mode NaCl-containing particles, although the likelihood is small. While passing over the Yellow Sea, these NaCl-containing particles might have been mixed with SSAs, as it was difficult to identify them in samples S2 and S3 by low-Z particle EPMA.

Notably, there were many (C, N, O, S)-rich particles in samples S2 and S3 (Figs. 5 and 8), whereas none were observed in sample S1, suggesting that the (C, N, O, S)-rich particles were formed favorably in Incheon. Besides $(NH_4)_2SO_4$ and water-soluble organic matter, NH_4NO_3 is also likely to be included in the (C, N, O, S)-rich particles as NH_4NO_3 is water-soluble and the measured N levels were sometimes

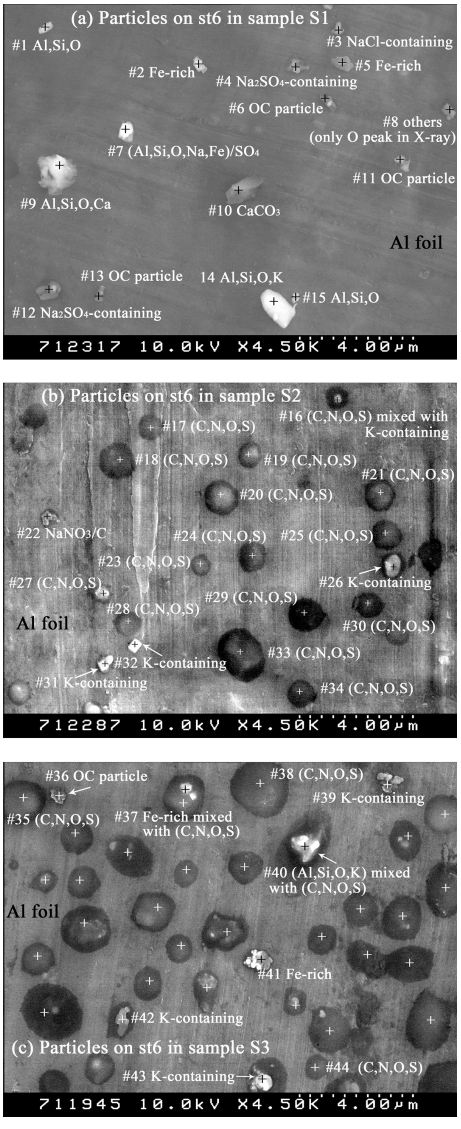

Fig. 5. SEIs of typical particles on stage 6 in samples S1, S2, and S3. (For Fig. 5c, those with a "+" are all particles rich in C, N, O, and S.)

higher than S levels (Fig. 11). Herein, the (C, N, O, S)-rich particles had higher abundance on stage 6 in samples S2 and S3 and were barely encountered on the other stages (except on stage 5 in sample S3, with 8.3 % in abundance), suggesting that they were small in size and generated in the high-humidity atmospheric environment, likely becoming droplets in the air. On the other hand, OC-containing particles on stage 6 were more abundant in sample S1 than samples S2 and S3 (23.6 % vs. 7.7 % and 9.6 %). Possibly, they dissolved in water and were absorbed into the (C, N, O, S)-containing droplet particles during transport when they passed over the sea.

K-containing particles, mostly from biomass burning (Wang et al., 2007; Liu et al., 2000, 2005), were encountered

Table 6. The concentrations of elements Na, N, S, and Cl and their ratios in the reacted SSAs at different stages in samples S2 and S3.

	Sample S2									Sample S3								
	Atomic concentration of elements (%)					Ratio of element atomic concentration				Atomic concentration of elements (%)					Ratio of element atomic concentration			
(1) Nitrate-containing																		
Size	*n*	Na	N	S	Cl	[Cl] / [Na]	[Cl] / [N]	[Cl] / [S]	[S] / [Na]	*n*	Na	N	S	Cl	[Cl] / [Na]	[Cl] / [N]	[Cl] / [S]	[S] / [Na]
st1	1	17	18		0	0	0			0								
st2	47	13	17		2	0.15	0.12			17	12	14		3	0.25	0.21		
st3	48	10	17		2	0.20	0.12			26	22	17		1	0.05	0.06		
st4	62	13	15		2	0.15	0.13			29	18	17		1	0.06	0.06		
st5	56	16	12		2	0.13	0.17			3	16	12		0	0	0		
ave		14	16		2	0.13	0.11				17	15		1	0.09	0.08		
(2) Sulfate-containing																		
st1	1	17		2	4	0.24		2	0.12	0								
st2	1	16		6	0	0		0	0.38	1	8		12	0	0		0	1.5
st3	0									3	8		12	1	0.13		0.08	1.5
st4	1	9		11	0	0		0	1.22	29	12		11	1	0.08		0.09	0.92
st5	2	16		8	0	0		0	0.50	4	18		7	0	0		0	0.39
ave		15		7	1	0.06		0.50	0.55		12		11	1	0.05		0.04	1.08
(3) Both-containing																		
st1	1	19	3	11	1	0.05	0.33	0.09	0.58	0								
st2	9	10	11	5	2	0.20	0.18	0.40	0.50	10	11	7	7	1	0.09	0.14	0.14	0.64
st3	19	9	9	5	1	0.11	0.11	0.20	0.56	23	15	10	5	1	0.07	0.10	0.20	0.33
st4	8	8	10	5	0	0	0	0	0.63	39	14	10	6	1	0.07	0.10	0.17	0.43
st5	88	14	8	4	1	0.07	0.13	0.25	0.29	22	13	15	8	0	0	0	0	0.62
ave		12	8	6	1	0.09	0.15	0.19	0.51		13	11	7	1	0.06	0.09	0.13	0.50

only on stage 6. They were less abundant in sample S1 than in samples S2 and S3 (2.4 % vs. 15.4 % and 15.4 %).

3.4 Mixing and aging processes of ADS particles during long-range transport

The air mass backward trajectory shows that this ADS originated mainly from the Gobi Desert in Mongolia, passed over arid and semi-arid regions of China (including the Inner Mongolia Autonomous Region and Hebei Province), and arrived at Beijing (Fig. 3). The ADS particles then passed over the Yellow Sea and reached Incheon. The time they spent over the Yellow Sea was approximately 5–8 h. This means that there was sufficient time for ADS particles to be mixed with SSAs or react with airborne pollutants. The low-Z particle EPMA measurement provides a strong indication of an aging process of ADS particles during long-range transport. Figure 12 illustrates their production, transport, growth, coagulation, and deposition (or collection) of ADS particles. Initially, when the ADS event started, a large number of mineral dust particles were uplifted and suspended in the air, resulting in a dramatically increased mass concentration of ambient particulate matter in the dust source area. These particles, which were comprised mostly of minerals, such as calcite, quartz, montmorillonite, feldspars, cristobalite, muscovite, and vermiculite, were transported by strong westerly winds to the middle and eastern areas of China, where anthropogenic air pollutants (e.g., SO_2, NO_2, NH_3, soot, and organic matters) from power plants, motor vehicles, cooking, biomass and/or fossil-fuel burning, etc. were emitted (Lee et al., 2013; Li et al., 2014). Reactive gases (e.g., SO_2, NO_2, etc.) were likely adsorbed on some of the dust particles and then oxidized to their acidic forms (e.g., HNO_3 and H_2SO_4), which would be neutralized fully or partially by the alkaline species (e.g., $CaCO_3$ or Ca/Mg-containing aluminosilicates) or by ambient NH_3 (Huang et al., 2010; Li and Shao, 2012); sometimes, ammonium salts or secondary aerosols (e.g., NH_4NO_3 and $(NH_4)_2SO_4$) would be adsorbed directly on dust particles (Manktelow et al., 2010; Formenti et al., 2011). When dust particles from the ADS event left the continent and entered the marine region atmosphere, they likely would have experienced significant modification by the surface uptake of gaseous species and mixing with fresh or aged (reacted) SSAs, rapidly becoming a mixture of mineral, SSA, sulfate, and/or nitrate in the marine atmosphere (Fan et al., 1996). Moisture over the sea is favorable not only for the reaction of mineral dust with airborne NO_x and SO_2 (resulting in more efficient transformation of SO_2 to sulfate and NO_x to nitrate) (Tursic et al., 2003), but also for the formation of (C, N, O, S)-rich particles, which are likely mixtures of NH_4NO_3 and $(NH_4)_2SO_4$ / NH_4HSO_4 with water-soluble organic carbon (WSOC). Previous studies have shown that nitrate formation is favored on aluminosilicates and $CaCO_3$ compared to sulfate (Ma et al., 2012; Li et al., 2012, 2014), which is consistent with our observation, i.e., most of reacted (or aged) mineral dust contained nitrates. In addition, nearly no fresh SSA particles were encountered and the majority of reacted SSA particles were $NaNO_3$-containing ones (the

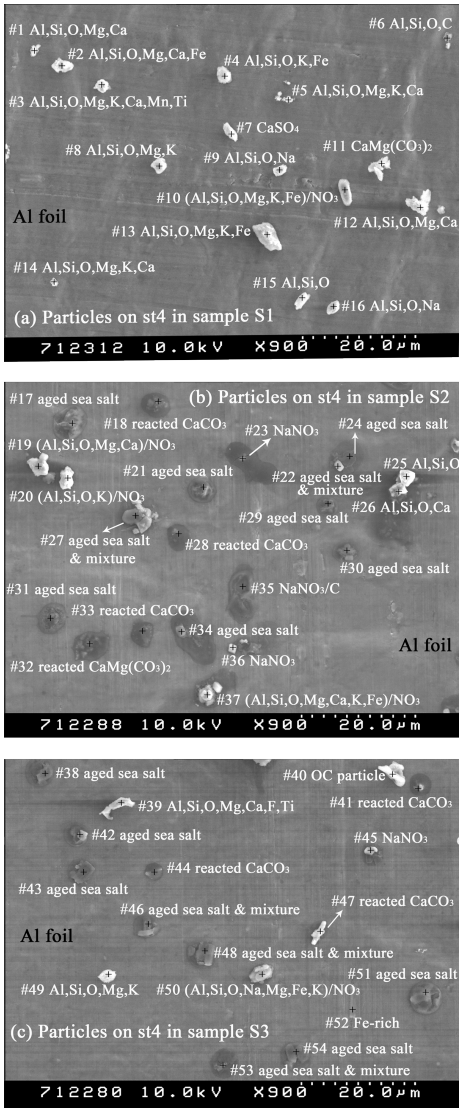

Fig. 6. SEIs of typical particles on stage 4 in samples S1–S3.

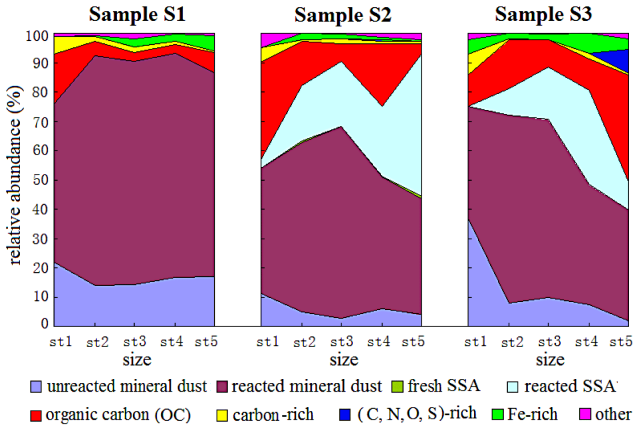

Fig. 7. Relative abundance percentages of various types of particles on stages 1–5 in samples S1–S3.

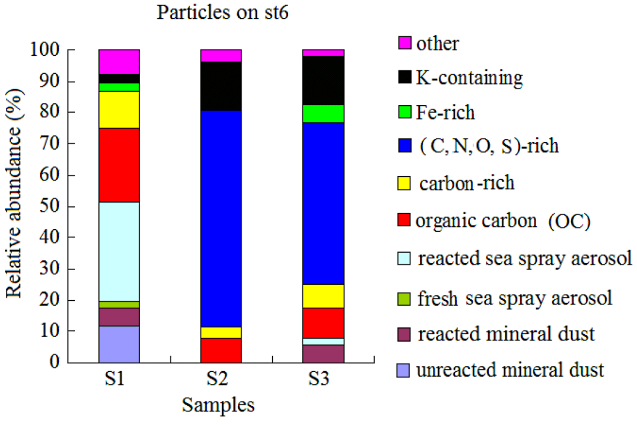

Fig. 8. Relative abundance percentages of various types of particles on stage 6 in samples S1–S3.

atomic concentration ratios of [Cl] / [N] and [Cl] / [Na] in the reacted nitrate-containing SSAs were in 0–0.21 and 0–0.25, respectively; see Table 6), indicating that the Cl depletion from SSAs was caused mostly by the uptake of HNO_3 (or NO_x) rather than that of H_2SO_4 (or SO_2).

The mixing of dust aerosols and SSAs is regarded as a likely and important process in composition change of ADS particles during long-range transport (Ma et al., 2004; Zhang et al., 2003). For SSA particles collected in Incheon, more than 60 % of them were internally mixed with mineral dust (Fig. 10), suggesting that the mixing of mineral dust and SSAs was rather routine. For mineral dust, the elevated [Mg] / [Al] and [Mg] / [Si] ratios in Mg-containing aluminosilicates of samples S2 and S3 (compared to those in sample S1) also suggest an accumulation of the sea-salt component on individual ADS particles over the Yellow Sea during transport. The mixtures of dust and SSA particles have been observed at several locations of Korea and Japan (such as Nagasaki and Kumamoto in Japan, and Incheon and Chuncheon in Korea) as well as over the ocean (such as the Yellow Sea) by other studies (Arimoto et al., 2006; Sullivan et al., 2007; Ma et al., 2004; Kojima et al., 2006; Hwang et al., 2008; Geng et al., 2009a; Fan et al., 1996; Niimura et al., 1998; Zhang et al., 2003; Okada et al., 1990; Andreae et al., 1986). Although the mechanisms responsible for the mixing of dust particles and SSAs have not been elucidated in detail (Zhang et al., 2006), particle-to-particle collisions and in-cloud processing are likely to be major ways for formation of the agglomerate (Ma, 2010; Li et al., 2012).

Figure 13 illustrates three types of mixing status of mineral dust particles and SSAs. A large mineral dust particle can interact with small SSA particles (or a large amount of dust particles can interact with a small amount of SSAs) (Type 1), a mineral dust particle can interact with a SSA particle of a comparable size (Type 2), and small mineral dust particles can interact with a large SSA particle (or a small

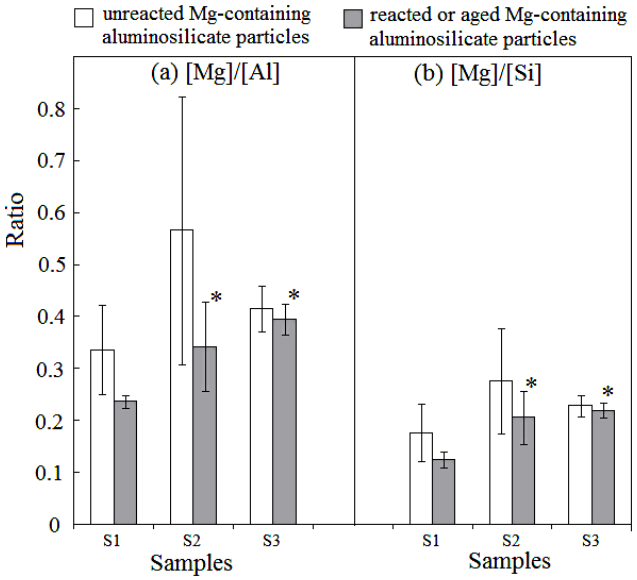

Fig. 9. Atomic concentration ratios of [Mg] / [Al] and [Mg] / [Si] for unreacted and reacted aluminosilicate particles in samples S1–S3 (Note: for the unreacted aluminosilicate particles, 182 Mg-containing species were considered; and for the reacted or aged ones, 1152 Mg-containing species were considered. Statistical comparisons of [Mg] / [Al] or [Mg] / [Si] ratios between samples S1 and S2 and between samples S1 and S3 were done by a student's *t* test. When the difference is statistically significant at $p < 0.05$, it is marked by an "*".).

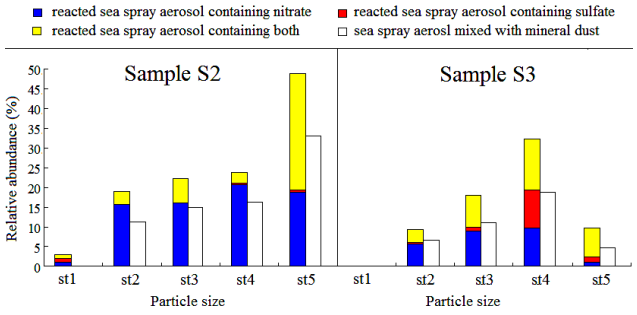

Fig. 10. Relative abundance percentages of various types of reacted SSAs (and mixture) in samples S2 and S3.

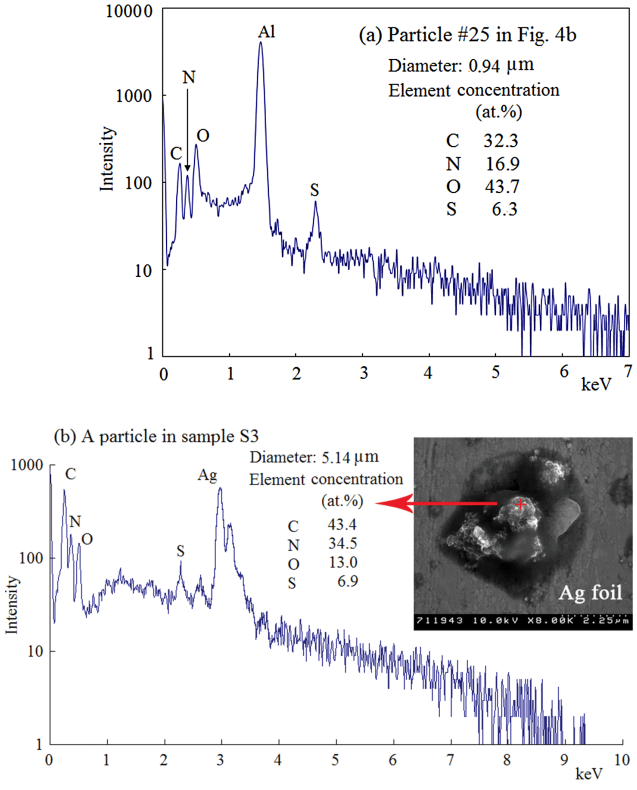

Fig. 11. Typical (C, N, O, S)-rich particles. **(a)** A typical particle collected on Al foil and **(b)** a typical particle collected on Ag foil (N concentration is relatively high).

amount of dust particles can interact with a large amount of SSAs) (Type 3). When a mineral dust particle is enclosed by SSA particles or a small mineral dust particle is coagulated with a large SSA particle, this type of mixture (Type 3) mainly consists of reacted sea salts as well as minor mineral dust, likely including components of $NaNO_3$, $Mg(NO_3)_2$, Na_2SO_4, $MgSO_4$, SiO_2, aluminosilicate, etc., which is classified as "reacted SSA and mixture" (as shown in Sect. 3.3.1 and Fig. 10). On the other hand, the coagulation of a large mineral dust particle with small SSA particles (Type 1) or dust and SSA particles of a comparable size (Type 2) result in the formation of a mineral dust particle mixed with SSA components. Given that aluminosilicates (of which Mg-containing species account for more than 50 % on average by number) are the main fraction of mineral dust, the interaction of Mg-containing aluminosilicate particles with reacted SSAs can lead to their elevated Mg and Na levels, as Mg-containing aluminosilicates were observed with the increase of atomic concentration ratios of [Mg] / [Al] and [Mg] / [Si] in samples S2 and S3. The frequent observation of Na signals for this type of particles supports that the increased Mg was due to the mixing of Mg-containing aluminosilicates and reacted SSAs. Because the Mg-containing aluminosilicates are an important part of ADS particles, the modification of the atomic concentration ratios of [Mg] / [Al] and [Mg] / [Si] likely reflected the aging of mineral dust when the ADS particles passed over the marine atmosphere.

4 Conclusions

Overall, 4200 individual particles in three sets of Asian dust storm (ADS) particle samples collected in Beijing, China (sample S1) and Incheon, Korea (samples S2 and S3) on 28–29 April 2005 were examined by low-*Z* particle EPMA. The morphology, elemental compositions, and mixing state of the particles on stages 1–6 with respective cut-off diameters of

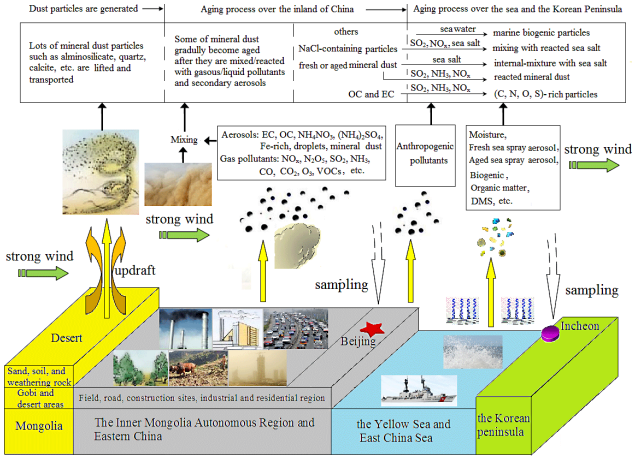

Fig. 12. Illustration of mixing and aging processes of Asian dust particles during long-range transport.

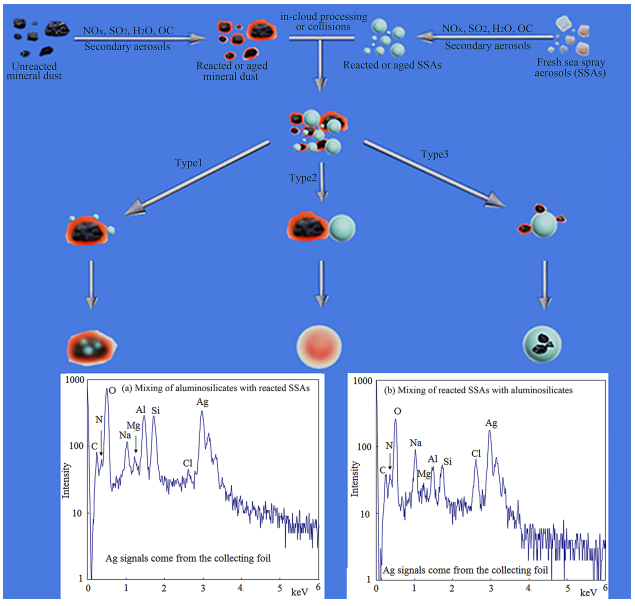

Fig. 13. Formation process of the coagulation of mineral dust with sea spray aerosols (SSAs).

16, 8, 4, 2, 1, and 0.5 µm were analyzed. Results showed that approximately 97 % of the analyzed particles were in the size range of 0.5–16 µm and there were extensive modification of ADS particles in chemical compositions during long-range transport from China to Korea. In addition to anthropogenic SO_2 and NO_x, SSAs in the marine atmosphere made great influences on the compositional change of ADS particles. For ADS particles larger than 1 µm (at stages 2–5) in sample S1, aged or reacted mineral dust were most abundant, followed by unreacted mineral dust, carbonaceous, and Fe-rich particles (no SSAs were detected). When the ADS passed over the sea, the dust particles were mixed with fresh or reacted SSAs. Approximately 24 % of aged or reacted SSAs (and the mixture with mineral dust) in sample S2 and 14 % in sample S3 were detected. Nitrate-containing and both nitrate- and sulfate-containing species in the reacted/aged mineral dust and SSAs outnumbered only sulfate-containing species, suggesting that ambient NO_x had a greater impact on ADS particles than SO_2 in this area. Besides partially or totally reacted $CaCO_3$, a number of reacted or aged Mg-containing aluminosilicates were encountered during the ADS event. The significant increase ($P < 0.05$ by a student's t test) of the atomic concentration ratios of [Mg] / [Al] and [Mg] / [Si] in the reacted Mg-containing aluminosilicates for samples 2 and 3 (compared to sample S1) was indicative of coagulation of Mg-containing aluminosilicates with SSAs, implying that a significant evolution or aging occurred on the mineral dust particles when they passed over the sea. The most obvious characteristic for the particles less than 1 µm in equivalent diameter (at stage 6) was that many (C, N, O, S)-rich particles (likely mixtures of $(NH_4)_2SO_4$ / NH_4HSO_4 and NH_4NO_3 with water-soluble organic carbon) were encountered (approximately 68 % and 51 % of relative number abundance in samples S2 and S3, respectively). This suggests that marine air likely facilitated the formation of secondary aerosols when ADS plumes passed over the sea, resulting in chemical composition change of ADS particles.

This study provides details of ADS particles that experienced extensive chemical modification during their dispersion from Beijing to Incheon in the marine atmosphere. As it appears that ADS particles can be modified greatly by SSAs through coagulations or in-cloud processing, further studies are needed for the full understanding on how the internal mixture of ADS particles with SSAs is formed and how anthropogenic air pollutants are incorporated into these dust and marine particles.

Acknowledgements. This study was supported by Basic Science Research Programs through the National Research Foundation of Korea (NRF) funded by the Ministry of Education, Science, and Technology (grant 2012R1A2A1A05026329) and by the National Natural Science Foundation of China (NSFC) (21177078) and NSFC-NRF Scientific Cooperation Program (grants 2012K1A2B1A03000431 and 41211140241). In addition, the authors gratefully acknowledge the support of Metrology Research Center funded by the Korea Research Institute of Standards and Science (KRISS-2013-13011055).

Edited by: A. Laskin

References

Andreae, M. O., Charlson, R. J., Bruynseels, F., Storms, H., Van Grieken, R., and Maenhaut, W.: Internal mixture of sea salt, silicates, and excess sulfate in marine aerosols, Science, 232, 1620–1623, 1986.

Arimoto, R., Kim, Y. J., Kim, Y. P., Quinn, P. K., Bates, T. S., Anderson, T. L., Gong, S., Uno, I., Chin, M., Huebert, B. J., Clarke, A. D., Shinozuka, Y., Weber, R. J., Anderson, J. R., Guazzotti, S. A., Sullivan, R. C., Sodeman, D. A., Prather, K. A., and Sokolik, I. N.: Characterization of Asian Dust during ACE-Asia, Global Planet. Change, 52, 23–56, 2006.

Atkinson, R.: Atmospheric chemistry of VOCs and NO_x, Atmos. Environ., 34, 2063–2101, 2000.

Ault, A. P., Moffet, R. C., Baltrusaitis, J., Collins, D. B., Ruppel, M. J., Cuadra-Rodriguez, L. A., Zhao, D., Guasco, T. L., Ebben, C. J., Geiger, F. M., Bertram, T. H., Prather K. A., and Grassian V. H.: Size-dependent changes in sea spray aerosol composition and properties with different seawater conditions, Environ. Sci. Technol., 47, 5603–5612, 2013.

Bauer, S. E., Mishchenko, M. I., Lacis, A. A., Zhang, S., Perlwitz, J., and Metzger, S. M.: Do sulfate and nitrate coatings on mineral dust have important effects on radiative properties and climate modeling?, J. Geophys. Res., 112, D06307, doi:10.1029/2005JD006977, 2007.

Choël, M., Deboudt, K., Osán, J., Flament, P., and Van Grieken, R.: Quantitative determination of low-Z elements in single atmospheric particles on boron substrates by automated scanning electron microscopy-energy-dispersive X-ray spectrometry, Anal. Chem., 77, 5686–5692, 2005.

Choël, M., Deboudt, K., and Flament, P.: Evaluation of quantitative procedures for X-ray microanalysis of environmental particles, Microsc. Res. Techniq., 70, 996–1002, 2007.

Choi, J. C., Lee, M., Chun, Y., Kim, J., and Oh, S.: Chemical composition and source signature of spring aerosol in Seoul, Korea, J. Geophys. Res., 106, 18067–18074, 2001.

Fairlie, T. D., Jacob, D. J., Dibb, J. E., Alexander, B., Avery, M. A., van Donkelaar, A., and Zhang, L.: Impact of mineral dust on nitrate, sulfate, and ozone in transpacific Asian pollution plumes, Atmos. Chem. Phys., 10, 3999–4012, doi:10.5194/acp-10-3999-2010, 2010.

Fan, X.-B., Okada, K., Niimura, N., Kai, K., Arao, K., Shi, G.-Y., Qin, Y., and Mitsuta, Y.: Mineral particles collected in China and Japan during the same Asian dust-storm event, Atmos. Environ., 30, 347–351, 1996.

Feng, Q., Endo, K. N., and Cheng, G. D.: Dust storms in China: a case study of dust storm variation and dust characteristics, B. Eng. Geol. Environ., 61, 253–261, 2002.

Flament, P., Mattielli, N., Aimoz, L., Choël, M., Deboudt, K., de Jong, J., Rimetz-Planchon, J., and Weis, D.: Iron isotopic fractionation in industrial emissions and urban aerosols, Chemosphere, 73, 1793–1798, 2008.

Formenti, P., Rajot, J. L., Desboeufs, K., Saïd, F., Grand, N., Chevaillier, S., and Schmechtig, C.: Airborne observations of mineral dust over western Africa in the summer Monsoon season: spatial and vertical variability of physico-chemical and optical properties, Atmos. Chem. Phys., 11, 6387–6410, doi:10.5194/acp-11-6387-2011, 2011.

Geng, H., Park, Y., Hwang, H., Kang, S., and Ro, C.-U.: Elevated nitrogen-containing particles observed in Asian dust aerosol samples collected at the marine boundary layer of the Bohai Sea and the Yellow Sea, Atmos. Chem. Phys., 9, 6933–6947, doi:10.5194/acp-9-6933-2009, 2009a.

Geng, H., Jung, H.-J., Park, Y., Hwang, H., Kim, H., Kim, Y. J., Sunwoo, Y., and Ro, C.-U.: Morphological and chemical composition characteristics of summertime atmospheric particles collected at Tokchok Island, Korea, Atmos. Environ., 43, 3364–3373, 2009b.

Geng, H., Cheng, F., and Ro, C.-U.: Single-particle characterization of atmospheric aerosols collected at Gosan, Korea, during the Asian Pacific Regional Aerosol Characterization Experiment Field Campaign using low-Z particle electron probe X-ray microanalysis, J. Air. Waste. Manage., 61, 1183–1191, doi:10.1080/10473289.2011.604292, 2011a.

Geng, H., Ryu, J. Y., Maskey, S., Jung, H.-J., and Ro, C.-U.: Characterisation of individual aerosol particles collected during a haze episode in Incheon, Korea using the quantitative ED-EPMA technique, Atmos. Chem. Phys., 11, 1327–1337, doi:10.5194/acp-11-1327-2011, 2011b.

Harris, E., Sinha, B., Foley, S., Crowley, J. N., Borrmann, S., and Hoppe, P.: Sulfur isotope fractionation during heterogeneous oxidation of SO_2 on mineral dust, Atmos. Chem. Phys., 12, 4867–4884, doi:10.5194/acp-12-4867-2012, 2012.

Hatch, C. D. and Grassian, V. H.: 10th Anniversary Review: Applications of analytical techniques in laboratory studies of the chemical and climatic impacts of mineral dust aerosol in the Earth's atmosphere, J. Environ. Monitor., 10, 919–934, 2008.

Hopkins, R. J., Desyaterik, Y., Tivanski, A. V., Zaveri, R. A., Berkowitz, C. M., Tyliszczak, T., Gilles, M. K., and Laskin, A.: Chemical speciation of sulfur in marine cloud droplets and particles: Analysis of individual particles from the marine boundary layer over the California current, J. Geophys. Res., 113, D04209, doi:10.1029/2007JD008954, 2008.

Huang, K., Zhuang, G. S., Li, J. A., Wang, Q. Z., Sun, Y. L., Lin, Y. F., and Fu, J. S.: Mixing of Asian dust with pollution aerosol and the transformation of aerosol components during the dust storm over China in spring 2007, J. Geophys. Res., 115, D00K13, doi:10.1029/2009JD013145, 2010.

Hwang, H. and Ro, C.-U.: Single-particle characterization of four aerosol samples collected in ChunCheon, Korea, during Asian dust storm events in 2002, J. Geophys. Res., 110, D23201, doi:10.1029/2005JD006050, 2005.

Hwang, H. and Ro, C.-U.: Direct observation of nitrate and sulfate formations from mineral dust and sea-salts using low-Z particle electron probe X-ray microanalysis, Atmos. Environ., 40, 3869–3880, 2006.

Hwang, H., Kim, H., and Ro, C.-U.: Single-particle characterization of aerosol samples collected before and during an Asian dust storm in Chuncheon, Korea, Atmos. Environ., 42, 8738–8746, 2008.

Huebert, B. J., Bates, T., Russell, P. B., Shi, G. Y., Kim, Y. J., Kawamura, K., Carmichael, G., and Nakajima, T.: An overview of ACE-Asia: Strategies for quantifying the relationships between Asian aerosols and their climatic impacts, J. Geophys. Res., 108, 8633, doi:10.1029/2003JD003550, 2003.

Iziomon, M. G., Lohmann, U., and Quinn, P. K.: Summertime pollution events in the Arctic and potential implications, J. Geophys. Res., 111, D12206, doi:10.1029/2005JD006223, 2006.

Jung, H., Malek, M. A., Ryu, J., Kim, B., Song, Y., Kim, H., and Ro, C.-U.: Speciation of individual mineral particles of micrometer size by the combined use of attenuated total reflectance-Fourier transform-infrared imaging and quantitative energy-dispersive electron probe X-ray microanalysis techniques, Anal. Chem., 82, 6193–6202, doi:10.1021/ac101006h, 2010.

Kojima, T., Buseck, P. R., Wilson, J. C., Reeves, J. M., and Mahoney, M. J.: Aerosol particles from tropical convective systems: Cloud tops and cirrus anvils, J. Geophys. Res., 109, D12201, doi:10.1029/2003JD004504, 2004.

Kojima, T., Buseck, P. R., Iwasaka, Y., Matsuki, A., and Trochkine, D.: Sulfate-coated dust particles in the free troposphere over Japan, Atmos. Res., 82, 698–708, 2006.

Krueger, B. J., Grassian, V. H., Laskin, A., and Cowin, J. P.: The transformation of solid atmospheric particles into liquid droplets through heterogeneous chemistry: Laboratory insights into the processing of calcium containing mineral dust aerosol in the troposphere, Geophys. Res. Lett., 30, 1148, doi:10.1029/2002GL016563, 2003.

Lee, S., Ho, C.-H., Lee, Y.G., Choi, H.-J., and Song, C.-K.: Influence of transboundary air pollutants from China on the high-PM_{10} episode in Seoul, Korea for the period October 16–20, 2008, Atmos. Environ., 77, 430–439, 2013.

Li, J., Wang, Z., Zhuang, G., Luo, G., Sun, Y., and Wang, Q.: Mixing of Asian mineral dust with anthropogenic pollutants over East Asia: a model case study of a super-duststorm in March 2010, Atmos. Chem. Phys., 12, 7591–7607, doi:10.5194/acp-12-7591-2012, 2012.

Li, W., Shao, L., Shi, Z., Chen, J., Yang, L., Yuan, Q., Yan, C., Zhang, X., Wang, Y., Sun, J., Zhang, Y., Shen, X., Wang, Z., and Wang, W.: Mixing state and hygroscopicity of dust and haze particles before leaving Asian continent, J. Geophys. Res., 119, 1044–1059, doi:10.1002/2013JD021003, 2014.

Li, W. J. and Shao, L. Y.: Observation of nitrate coatings on atmospheric mineral dust particles, Atmos. Chem. Phys., 9, 1863–1871, doi:10.5194/acp-9-1863-2009, 2009.

Li, W. J. and Shao, L. Y.: Chemical modification of dust particles during different dust storm episodes, Aerosol Air Qual. Res., 12, 1095–1104, doi:10.4209/aaqr.2011.11.0188, 2012.

Liu, X., Van Espen, P., Adams, F., Cafmeyer, J., and Maenhaut, W.: Biomass burning in Southern Africa: Individual particle characterization of atmospheric aerosols and savanna fire samples, J. Atmos. Chem., 36, 135–155, 2000.

Liu, X., Zhu, J., Van Espen, P., Adams, F., Xiao, R., Dong, S., and Li, Yu.: Single particle characterization of spring and summer aerosols in Beijing: Formation of composite sulfate of calcium and potassium, Atmos. Environ., 39, 6909–6918, 2005.

Liu, Z. Y., Fairlie, T. D., Uno, I., Huang, J. F., Wu, D., Omarb, A., Kar, J., Vaughan, M., Rogers, R., Winker, D., Trepte, C., Hu, Y. X., Sun, W. B., Lin, B., and Cheng, A. N.: Transpacific transport and evolution of the optical properties of Asian dust, J. Quant. Spectrosc. Ra., 116, 24–33, 2013.

Ma, C. J.: Chemical transformation of individual Asian Dust particles estimated by the novel double detector system of Micro-PIXE, Asian J. Atmos. Environ., 4, 106–114, doi:10.5572/ajae.2010.4.2.106, 2010.

Ma, C. J., Tohno, S., Kasahara, M., and Hayakawa, S.: Properties of individual Asian dust storm particles collected at Kosan, Korea during ACE-Asia, Atmos. Environ., 38, 1133–1143, 2004.

Ma, Q., Liu, Y., Liu, C., Ma, J., and He, H.: A case study of Asian dust storm particles: chemical composition, reactivity to SO_2 and hygroscopic properties, J. Environ. Sci., 24, 62–71, 2012.

Malek, M. A., Kim, B., Jung, H., Song, Y., and Ro, C.-U.:Single-particle mineralogy of Chinese soil particles by the combined use of low-Z particle electron probe X-ray microanalysis and attenuated total reflectance-FT-IR imaging techniques, Anal. Chem., 83, 7970–7977, doi:10.1021/ac201956h, 2011.

Manktelow, P. T., Carslaw, K. S., Mann, G. W., and Spracklen, D. V.: The impact of dust on sulfate aerosol, CN and CCN during an East Asian dust storm, Atmos. Chem. Phys., 10, 365–382, doi:10.5194/acp-10-365-2010, 2010.

Maskey, S., Choël, M., Kang, S., Hwang, H., Kim, H., and Ro, C.-U.: The influence of collecting substrates on the single-particle characterization of real atmospheric aerosols, Anal. Chim. Acta, 658, 120–127, doi:10.1016/j.aca.2009.11.006, 2010.

Maskey, S., Geng, H., Song, Y., Hwang, H., Yoon, Y., Ahn, K., and Ro, C.-U.: Single-particle characterization of summertime Antarctic aerosols collected at King George Island using quantitative energy-dispersive electron probe X-ray microanalysis and attenuated total reflection Fourier transform-infrared imaging techniques, Environ. Sci. Technol., 45, 6275–6282, doi:10.1021/es200936m, 2011.

Matsumoto, J., Takahashi, K., Matsumi, Y., Yabushita, A., Shimizu, A., Matsui, I., and Sugimoto, N.: Scavenging of pollutant acid substances by Asian mineral dust particles, Geophys. Res. Lett., 33, L07816, doi:10.1029/2006GL025782, 2006.

Mori, I., Nishikawa, M., Tanimura, T., and Quan, H.: Change in size distribution and chemical composition of kosa (Asian dust) aerosol during long-range transport, Atmos. Environ., 37, 4253–4263, 2003.

Natsagdorj, L., Jugder, D., and Chung, Y. S.: Analysis of dust storms observed in Mongolia during 1937–1999, Atmos. Environ., 37, 1401–1411, 2003.

Nie, W., Wang, T., Xue, L. K., Ding, A. J., Wang, X. F., Gao, X. M., Xu, Z., Yu, Y. C., Yuan, C., Zhou, Z. S., Gao, R., Liu, X. H., Wang, Y., Fan, S. J., Poon, S., Zhang, Q. Z., and Wang, W. X.: Asian dust storm observed at a rural mountain site in southern China: chemical evolution and heterogeneous photochemistry, Atmos. Chem. Phys., 12, 11985–11995, doi:10.5194/acp-12-11985-2012, 2012.

Niimura, N., Okada, K., Fan, X. B., Kai, K., Arao, K., Shi, G. Y., and Takahashi, S.: Formation of Asian dust-storm particles mixed internally with sea-salt in the atmosphere, J. Meteorol. Soc. Jpn., 76, 275–288, 1998.

Okada, K. and Kai, K.: Atmospheric Mineral Particles Collected at Qira in the Taklamakan Desert, China, Atmos. Environ., 38, 6927–6935, 2004.

Okada, K., Naruse, H., Tanaka, T., Nemoto, O., Iwasaka, Y., Wu, P. M., Ono, A., Duce, R. A., Uematsu, M., Merrill, J. T., and Arao, K.: X-ray spectrometry of individual Asian dust storm particles over the Japanese islands and the north Pacific Ocean, Atmos. Environ., 24, 1369–1378, 1990.

Ro, C.-U., Osan, J., Szaloaki, I., Oh, K. Y., and Van Grieken, R.: Determination of chemical species in individual aerosol particles using ultrathin window EPMA, Environ. Sci. Technol., 34, 3023–3030, 2000.

Ro, C.-U., Oh, K.-Y., Kim, H., Chun, Y.-S., Osan, J., de Hoog, J., and Van Grieken, R.: Chemical speciation of individual atmospheric particles using low-Z electron probe X-ray microanalysis: characterizing "Asian Dust" deposited with rainwater in Seoul, Korea, Atmos. Environ., 35, 4995–5005, 2001.

Ro, C.-U., Osán, J., Szalóki, I., de Hoog, J., Worobiec, A., and Van Grieken, R.: A Monte Carlo program for quantitative

electron-induced X-ray analysis of individual particles, Anal. Chem., 75, 851–859, 2003.

Ro, C.-U., Kim, H., and Van Grieken, R.: An expert system for chemical speciation of individual particles using low-Z particle electron probe X-ray microanalysis data, Anal. Chem., 76, 1322–1327, 2004.

Schulz, M., Prospero, J. M., Baker, A. R., Dentener, F., Ickes, L., Liss, P. S., Mahowald, N. M., Nickovic, S., García-Pando, C. P., Rodríguez, S., Sarin, M., Tegen, I., and Duce, R. A.: Atmospheric transport and deposition of mineral dust to the ocean: implications for research deeds, Environ. Sci. Technol., 46, 10390–10404, 2012.

Shao, L. Y., Li, W. J., Xiao, Z. H., and Sun, Z. Q.: The mineralogy and possible sources of spring dust particles over Beijing, Adv. Atmos. Sci., 25, 395–403, 2008.

Sobanska, S., Hwang, H., Choël, M., Jung, H., Eom, H., Kim, H., Barbillat, J., and Ro, C.-U.: Investigation of the chemical mixing state of individual Asian Dust particles by the combined use of electron probe X-ray microanalysis and Raman microspectrometry, Anal. Chem., 84, 3145–3154, doi:10.1021/ac2029584, 2012.

Song, Y.-C., Eom, H.-J., Jung, H.-J., Malek, M. A., Kim, H. K., Geng, H., and Ro, C.-U.: Investigation of aged Asian dust particles by the combined use of quantitative ED-EPMA and ATR-FTIR imaging, Atmos. Chem. Phys., 13, 3463–3480, doi:10.5194/acp-13-3463-2013, 2013.

Sullivan, R. C., Guazzotti, S. A., Sodeman, D. A., and Prather, K. A.: Direct observations of the atmospheric processing of Asian mineral dust, Atmos. Chem. Phys., 7, 1213–1236, doi:10.5194/acp-7-1213-2007, 2007.

Sun, Y., Zhuang, G., Huang, K., Li, J., Wang, Q., Wang, Y., Lin, Y., Fu, J. S., Zhang, W., Tang, A., and Zhao, X.: Asian dust over northern China and its impact on the downstream aerosol chemistry in 2004, J. Geophys. Res., 115, D00k09, doi:10.1029/2009JD012757, 2010.

Takahashi, H., Naoe, H., Igarashi, Y., Inomata, Y., and Sugimoto, N.: Aerosol concentrations observed at Mt. Haruna, Japan, in relation to long-range transport of Asian mineral dust aerosols, Atmos. Environ., 44, 4638–4644, 2010.

Tobo, Y., Zhang, D., Matsuki, A., and Iwasaka, Y.: Asian dust particles converted into aqueous droplets under remote marine atmospheric conditions, P. Natl. Acad. Sci. USA, 107, 17905–17910, 2010.

Tursic, J., Berner, A., Veber, M., Bizjak, M., Podkrajsek, B., and Grgic, I.: Sulfate formation on synthetic deposits under haze conditions, Atmos. Environ., 37, 3509–3516, 2003.

Usher, C. R., Michel, A. E., and Grassian, V. H.: Reactions on mineral dust, Chem. Rev., 103, 4883–4940, 2003.

Vekemans, B., Janssens, K., Vincze, L., Adams, F., and Van Espen, P.: Analysis of X-ray spectra by iterative least squares (AXIL): New developments, X-Ray Spectrom., 23, 278–285, 1994.

Wang, G. H., Zhou, B. H., Cheng, C. L., Cao, J. J., Li, J. J., Meng, J. J., Tao, J., Zhang, R. J., and Fu, P. Q.: Impact of Gobi desert dust on aerosol chemistry of Xi'an, inland China during spring 2009: differences in composition and size distribution between the urban ground surface and the mountain atmosphere, Atmos. Chem. Phys., 13, 819–835, doi:10.5194/acp-13-819-2013, 2013.

Wang, P. and Zhao, W.: Assessment of ambient volatile organic compounds (VOCs) near major roads in urban Nanjing, China, Atmos. Res., 89, 289–297, 2008.

Wang, Y., Zhuang, G. S., Sun, Y. L., and An, Z. S.: Water-soluble part of the aerosol in the dust storm season – evidence of the mixing between mineral and pollution aerosols, Atmos. Environ., 39, 7020–7029, 2005.

Xuan, J., Sokolik, I. N., Hao, J., Guo, F., Mao, H., and Yang, G.: Identification and characterization of sources of atmospheric mineral dust in East Asia, Atmos. Environ., 38, 6239–6252, 2004.

Yang, G. P., Zhang, H. H., Su, L. P., and Zhou, L. M.: Biogenic emission of dimethylsulfide (DMS) from the North Yellow Sea, China and its contribution to sulfate in aerosol during summer, Atmos. Environ., 43, 2196–2203, 2009.

Yuan, H., Zhuang, G., Rahn, K. A., Zhang, X., and Li, Y.: Composition and mixing of individual particles in dust and nondust conditions of north China, spring 2002, J. Geophys. Res., 111, D20208, doi:10.1029/2005JD006478, 2006.

Zhang, D. Z., Iwasaka, Y., Shi, G. Y., Zang, J. Y., Matsuki, A., and Trochkine, D.: Mixture state and size of Asian dust particles collected at southwestern Japan in spring 2000, J. Geophys. Res., 108, 4760, doi:10.1029/2003JD003869, 2003.

Zhang, D. Z., Iwasaka, Y., Matsuki, A., Ueno, K., and Matsuzaki, T.: Coarse and accumulation mode particles associated with Asian dust in southwestern Japan, Atmos. Environ, 40, 1205–1215, 2006.

Zhang, K., Chai, F. H., Zhang, R. J., and Xue, Z. G.: Source, route and effect of Asian sand dust on environment and the oceans, Particuology, 8, 319–324, 2010.